

Effect of yttrium substitution on the superconducting properties of the system $\text{La}_{1-x}\text{Y}_x\text{O}_{0.5}\text{F}_{0.5}\text{BiS}_2$

I. Jeon,^{1,2,3} D. Yazici,^{1,2} B. D. White,^{1,2} A. J. Friedman,^{1,2} and M. B. Maple^{1,2,3,*}

¹*Department of Physics, University of California, San Diego, La Jolla, California 92093, USA*

²*Center for Advanced Nanoscience, University of California, San Diego, La Jolla, California 92093, USA*

³*Materials Science and Engineering Program, University of California, San Diego, La Jolla, California 92093, USA*

We present the effect of yttrium substitution on superconductivity in the $\text{La}_{1-x}\text{Y}_x\text{O}_{0.5}\text{F}_{0.5}\text{BiS}_2$ system. Polycrystalline samples with nominal Y concentrations up to 40% were synthesized and characterized via electrical resistivity, magnetic susceptibility, and specific heat measurements. Y substitution reduces the lattice parameter a and unit cell volume V , and a correlation between the lattice parameter c , the La-O-La bond angle, and the superconducting critical temperature T_c is observed. The chemical pressure induced by Y substitution for La produces neither the high- T_c superconducting phase nor the structural phase transition seen in $\text{LaO}_{0.5}\text{F}_{0.5}\text{BiS}_2$ under externally applied pressure.

PACS numbers: 74.25.F-, 74.62.Dh, 74.62.Fj, 33.15.Dj

I. INTRODUCTION

Superconductivity was recently discovered in the layered compound $\text{Bi}_4\text{O}_4\text{S}_3$ with critical temperature $T_c = 8.6$ K[1,2]. Shortly thereafter, superconductivity was reported in fluorine-doped $\text{LnO}_{1-x}\text{F}_x\text{BiS}_2$ ($\text{Ln} = \text{La}, \text{Ce}, \text{Pr}, \text{Nd}, \text{Yb}$) compounds, with a maximum $T_c = 10.6$ K[3–12]. A layered structure is also observed for these materials, composed of superconducting BiS_2 and blocking oxide layers. Subsequent studies demonstrated that superconductivity is induced in general by electron doping in the blocking layers, as with the systems $\text{LnO}_{1-x}\text{F}_x\text{BiS}_2$ ($\text{Ln} = \text{La}, \text{Ce}, \text{Pr}, \text{Nd}, \text{Yb}$) and $\text{La}_{1-x}\text{M}_x\text{OBiS}_2$ ($M = \text{Ti}, \text{Zr}, \text{Hf}, \text{Th}$)[13], or doping in the isocharge block $[\text{Ln}_2\text{O}_2]^{2-}$ with a $[\text{Sr}_2\text{F}_2]^{2-}$ layer[14,15]. The parent compounds, AOBiS_2 ($A = \text{La}, \text{Ce}, \text{Th}$)[6,13] and SrFBiS_2 [14–16], are bad metals and show semiconducting-like behavior; however, theoretical studies employing the tight-binding model and density functional calculations predicted that electron doping in the BiS_2 system increases the density of states at the Fermi level[17,18], making electron doping a crucial tuning parameter for superconductivity. The pairing mechanism in both $\text{Bi}_4\text{O}_4\text{S}_3$ and $\text{LaO}_{0.5}\text{F}_{0.5}\text{BiS}_2$ has also been investigated; recent studies of the temperature dependence of the penetration depth by the tunnel diode oscillator technique revealed evidence for fully gapped, strongly-coupled s-wave superconductivity in the $\text{Bi}_4\text{O}_4\text{S}_3$ compound[19], and an s-wave character for $\text{LaO}_{0.5}\text{F}_{0.5}\text{BiS}_2$ was indicated in muon-spin spectroscopy measurements[20]. It has been suggested that superconductivity emerges in the vicinity of a charge-density wave (CDW) and semiconducting-like behavior[6, 21]. Moreover, neutron scattering measurements on the $\text{LaO}_{1-x}\text{F}_x\text{BiS}_2$ system show intrinsic structural instabilities in the superconducting phases[22]. As a consequence, studies focused on applied pressure as a tuning parameter in BiS_2 compounds have been conducted recently. It has been reported that the $\text{LnO}_{0.5}\text{F}_{0.5}\text{BiS}_2$

($\text{Ln} = \text{La}, \text{Ce}, \text{Pr}, \text{Nd}$) compounds show marked T_c enhancements[23–27] when subjected to applied pressure. A study of $\text{LaO}_{0.5}\text{F}_{0.5}\text{BiS}_2$ with various lattice parameters has shown that reducing the lattice parameters should have an effect on T_c [28]. To further investigate the relationships between pressure, lattice parameters, and superconductivity, chemical substitution of Y for La is a logical way to tune the properties of $\text{LaO}_{0.5}\text{F}_{0.5}\text{BiS}_2$. Like La, Y has no magnetic moment and a trivalent electronic configuration, and chemical pressure can be introduced by partial substitution of La by smaller Y ions. The effect of Y substitution has been studied for a number of superconducting systems, with suppression of superconductivity observed in the systems $(\text{La}_{1-x}\text{Y}_x)_{1.85}\text{Sr}_{0.15}\text{CuO}_4$ and $(\text{La}_{1-x}\text{Y}_x)\text{NiC}_2$ [29, 30], and enhancement of superconductivity observed in $(\text{La}_{1-x}\text{Y}_x)\text{Co}_2\text{B}_2$, $\text{La}_{1-x}\text{Y}_x\text{FeAsO}_{1-\delta}$, and F-doped $\text{La}_{1-y}\text{Y}_y\text{FeAsO}$ [31–33]. The latter system shows a remarkable enhancement of T_c from 24 K to 40 K. The effect of Y substitution on the BiS_2 systems has not been explored yet. In this work, we present a systematic study in which we have substituted Y ions into the La-site in $\text{LaO}_{0.5}\text{F}_{0.5}\text{BiS}_2$. We observe that the critical temperature T_c appears to be correlated with the lattice parameter c and the La-O-La bond angle. The chemical pressure resulting from Y substitution is insufficient to induce the structural phase transition from tetragonal ($P4/nmm$) to monoclinic ($P2_1/m$) crystal structures seen under an applied pressure of 1 GPa in $\text{LaO}_{0.5}\text{F}_{0.5}\text{BiS}_2$ [34].

II. EXPERIMENTAL DETAILS

Polycrystalline samples of $\text{La}_{1-x}\text{Y}_x\text{O}_{0.5}\text{F}_{0.5}\text{BiS}_2$ ($0 \leq x \leq 0.40$) were prepared by a conventional solid state reaction method. High-purity starting materials (purity $\geq 99.9\%$) of La, Y, and S, as well as LaF_3 , Bi_2O_3 , and Bi_2S_3 were weighed stoichiometrically. They were well-mixed, pressed into pellets, encapsulated in evacu-

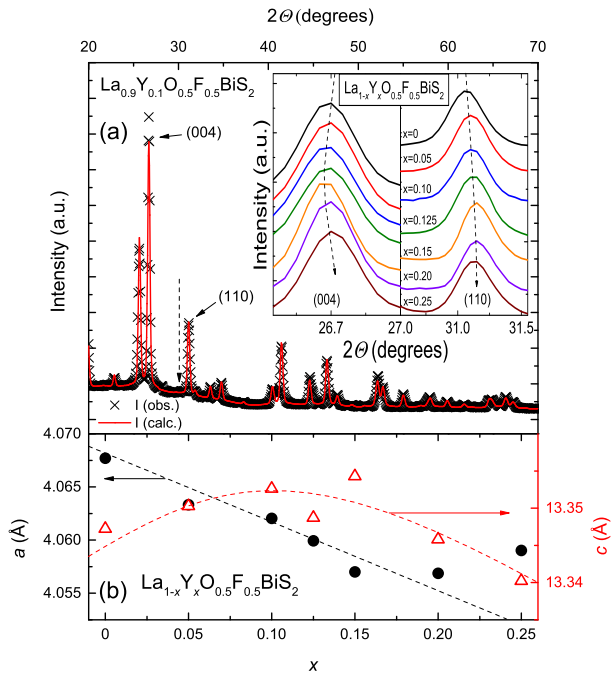


FIG. 1: (Color online) (a) X-ray diffraction pattern for $\text{La}_{0.9}\text{Y}_{0.1}\text{O}_{0.5}\text{F}_{0.5}\text{BiS}_2$. The black crosses are data and the red line represents the fit results from Rietveld refinement of the data. The dashed arrow indicates a $\text{La}_2\text{O}_2\text{S}$ and/or $\text{Y}_2\text{O}_2\text{S}$ impurity. The systematic behavior of the (004) and (110) diffraction peaks is shown in the inset of the graph. (b) Lattice parameters a and c versus nominal yttrium concentration x .

ated quartz tubes, and annealed at 800 °C for two days. This process was repeated two additional times to promote homogeneity of the samples. The crystal structure was determined by x-ray powder diffraction (XRD) using a Bruker D8 Discover x-ray diffractometer with Cu-K_α radiation and XRD patterns were analyzed via Rietveld refinement using the GSAS+EXPGUI software package[35,36]. The temperature dependence of electrical resistivity was measured from 1.1 K to 300 K using a standard four-wire method with a Linear Research LR700 ac resistance bridge and a home-built probe in a liquid ^4He Dewar. Magnetic susceptibility measurements were performed between 2 K and 10 K with applied magnetic field $H = 5$ Oe using a Quantum Design Magnetic Properties Measurement System (MPMS). Alternating current magnetic susceptibility was measured down to ~ 1.1 K in a liquid ^4He Dewar using home-built magnetic susceptibility coils. Specific heat measurements were made for $1.8 \text{ K} \leq T \leq 30 \text{ K}$ with a Quantum Design Physical Properties Measurement System (PPMS) DynaCool.

III. RESULTS

A. X-ray diffraction

Figure 1 shows XRD data for $\text{La}_{1-x}\text{Y}_x\text{O}_{0.5}\text{F}_{0.5}\text{BiS}_2$ ($0 \leq x \leq 0.25$) samples. All XRD patterns are well indexed by the tetragonal CeOBiS_2 -type crystal structure with space group $P4/nmm$. Figure 1 (a) displays the XRD pattern and the result of Rietveld refinement of the data for the $\text{La}_{0.9}\text{Y}_{0.1}\text{O}_{0.5}\text{F}_{0.5}\text{BiS}_2$ sample. The dashed arrow indicates the presence of $\text{La}_2\text{O}_2\text{S}$ and/or $\text{Y}_2\text{O}_2\text{S}$ impurity phases, the amount of which increases gradually with increasing x . This implies a possible minor discrepancy between nominal and actual yttrium concentrations. The samples with $x \leq 0.25$ contain the same impurity phase constituting 1%-8% of the sample by mass and less than 1% of possible Y and Bi/ Bi_2S_3 impurity phases by mass, as estimated by Rietveld refinements. The systematic behavior of the (004) and (110) diffraction peaks is shown in the inset of Fig. 1 (a) and the a and c lattice parameters are plotted as a function of nominal Y concentration in Fig. 1 (b).

To estimate the true Y concentration in our samples, we calculated the expected unit cell volume of $\text{YO}_{0.5}\text{F}_{0.5}\text{BiS}_2$ (which has thus far not been successfully synthesized) and then compared the measured volumes of our $\text{La}_{1-x}\text{Y}_x\text{O}_{0.5}\text{F}_{0.5}\text{BiS}_2$ samples against the expected behavior from Vegard's law. To estimate the unit cell volume of $\text{YO}_{0.5}\text{F}_{0.5}\text{BiS}_2$, we first calculated the total volume of the ions residing in a single unit cell of $\text{LaO}_{0.5}\text{F}_{0.5}\text{BiS}_2$ using ionic radii values of the elements from Ref. [37]. We then computed a scale factor by comparing the total volume of the ions with the measured unit cell volume of $\text{LaO}_{0.5}\text{F}_{0.5}\text{BiS}_2$. Assuming a similar scale factor is appropriate for the compounds containing other rare-earth ions, we made similar calculations to estimate their unit cell volumes. The trend of these estimated unit cell volumes for rare-earth ions is displayed in Fig. 2 (a) along with measured values for some compounds. Our estimate seems to work particularly well for $\text{CeO}_{0.5}\text{F}_{0.5}\text{BiS}_2$, but we note that there is a significant spread in experimentally-measured unit cell volumes for the other compounds and that our estimates are reasonable given such uncertainty. Invoking Vegard's law, we plot a line between the measured unit cell volume for $\text{LaO}_{0.5}\text{F}_{0.5}\text{BiS}_2$ and our estimated value for the volume of $\text{YO}_{0.5}\text{F}_{0.5}\text{BiS}_2$, and compare this line with the measured volumes of our $\text{La}_{1-x}\text{Y}_x\text{O}_{0.5}\text{F}_{0.5}\text{BiS}_2$ samples up to $x = 0.40$ in Fig. 2 (b). The agreement between measured and estimated volumes is good up to $x = 0.20$ and this simple procedure helps to get an idea of the uncertainty for the Y concentrations; the difference between nominal and estimated concentrations can be as large as 3% for the first batch of the $x = 0.10$ sample, for instance.

For $x \geq 0.25$, the unit cell volumes V are concentration-independent, as seen in Fig. 2 (b) and the XRD patterns contain impurity phases of Y, $\text{La}_2\text{O}_2\text{S}/\text{Y}_2\text{O}_2\text{S}$, and Bi/ Bi_2S_3 , suggesting that the sam-

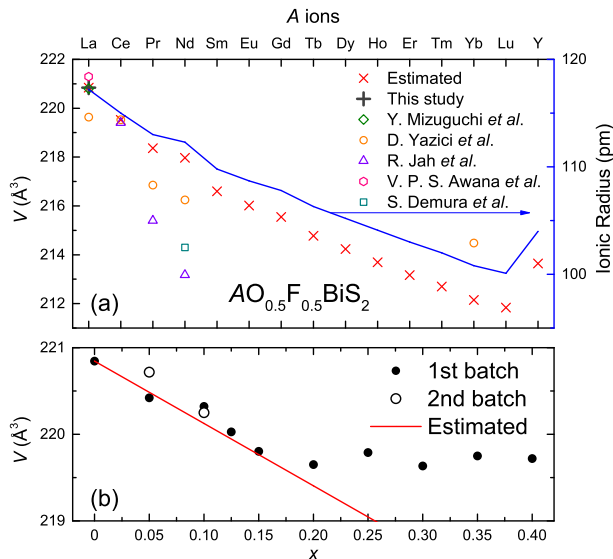


FIG. 2: (Color online) (a) Estimated volumes and ionic radii versus lanthanide and Y ions are shown for $\text{AO}_{0.5}\text{F}_{0.5}\text{BiS}_2$. The blue line is the trend of ionic radii for lanthanide and Y ions. Red crosses are estimated volumes and other symbols are reported volumes for $\text{LnO}_{0.5}\text{F}_{0.5}\text{BiS}_2$ ($\text{Ln} = \text{La}, \text{Ce}, \text{Pr}, \text{Nd}, \text{Yb}$). The estimated volume of $\text{YO}_{0.5}\text{F}_{0.5}\text{BiS}_2$ is at the right corner. (b) Black circles and red line are observed and estimated unit cell volumes V versus x , respectively. Unfilled circles correspond to a second batch of samples prepared for selected Y concentrations.

ple with $x = 0.25$ is near or even beyond the solubility limit. Therefore, we can conservatively conclude that Y is incorporated into the La site up to $x = 0.20$ in this system. Since the system forms with a tetragonal crystal structure ($P4/nmm$), the lattice parameter a has a more dominant effect than the lattice parameter c on the unit cell volume V , with both a and V decreasing with increasing x . Also, the ionic radius of Y is less than that of La, suggesting that chemical pressure is induced in $\text{La}_{1-x}\text{Y}_x\text{O}_{0.5}\text{F}_{0.5}\text{BiS}_2$ up to $x = 0.20$.

B. Electrical Resistivity

Electrical resistivity $\rho(T)$ data are plotted in Fig. 3. For all samples in their normal states, electrical resistivity exhibits semiconducting-like behavior and clear drops at the superconducting transition temperature T_c . We determined T_c by measuring the temperatures where the electrical resistivity falls to 50% of its normal-state value, and the broadness of the transitions was characterized by identifying the temperatures where the electrical resistivity decreases to 90% and 10% of the normal-state value. We observe two different types of behavior: for $x \leq 0.10$, ρ increases rapidly with decreasing temperature in its normal-state and a broad superconducting transition is observed, while a slower increase of ρ with

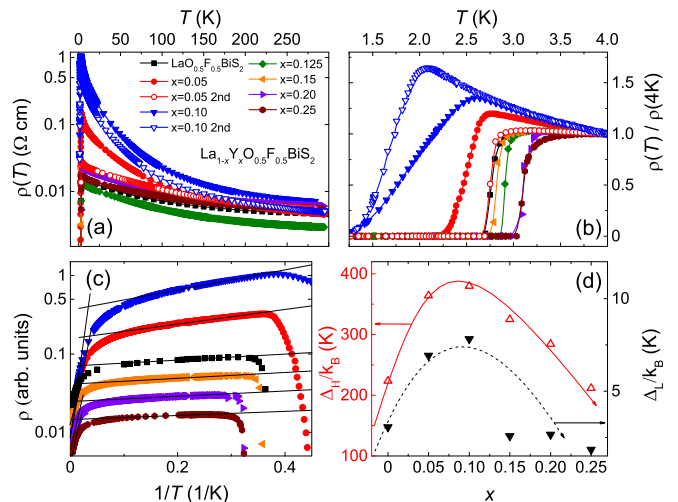


FIG. 3: (Color online) (a) A semilogarithmic plot of electrical resistivity ρ versus temperature T . (b) ρ , normalized to its value at 4 K, versus temperature T . (c) $\ln \rho$ versus $1/T$ for selected samples with $x = 0, 0.05, 0.10, 0.15, 0.20$, and 0.25 . The solid lines indicate simple activation-type temperature dependencies from Eq. (1). The data are vertically offset for visual clarity. (d) Energy gaps Δ_H/k_B and Δ_L/k_B calculated at high and low temperatures respectively, versus nominal yttrium concentration x .

decreasing temperature accompanying a sharp superconducting transition is seen for $x > 0.10$. Such behavior is emphasized by plotting $\rho(T)$, normalized by its value at 4 K, versus temperature T in Fig. 3 (b). To confirm the reproducibility of these different types of behavior, we have synthesized and characterized several additional samples for each Y concentration, especially for $x = 0.05$ and 0.10 . Since we observed the same behavior for different samples within all batches, shown in Figs. 2(b), 3(a) and (b), and 6(b), we only present representative data for each concentration in this study. To estimate the energy gaps, we adopted the simple activation-type relation[23],

$$\rho(T) = \rho_0 e^{\Delta/2k_B T}, \quad (1)$$

where ρ_0 is a constant and Δ is the energy gap. As shown in Fig. 3 (c), we fit Eq. 1 to data for selected samples in two regions, 200 - 300 K and $T_c - 20$ K, to obtain a high-temperature energy gap Δ_H/k_B and a low-temperature energy gap Δ_L/k_B , respectively. Both energy gaps are found to first increase with x up to $x = 0.10$ and then decrease with higher concentration, as illustrated in Fig. 3 (d). This behavior exhibits the same trend as that of the lattice parameter c . The behavior of the electrical resistivity up to $x = 0.10$ is different from that observed under applied external pressure on BiS_2 -based superconducting compounds[23–27,34], in which semiconducting-like behavior is suppressed with increasing pressure and a metallic state is induced. On the other hand, we note that there is currently no data for applied pressures less

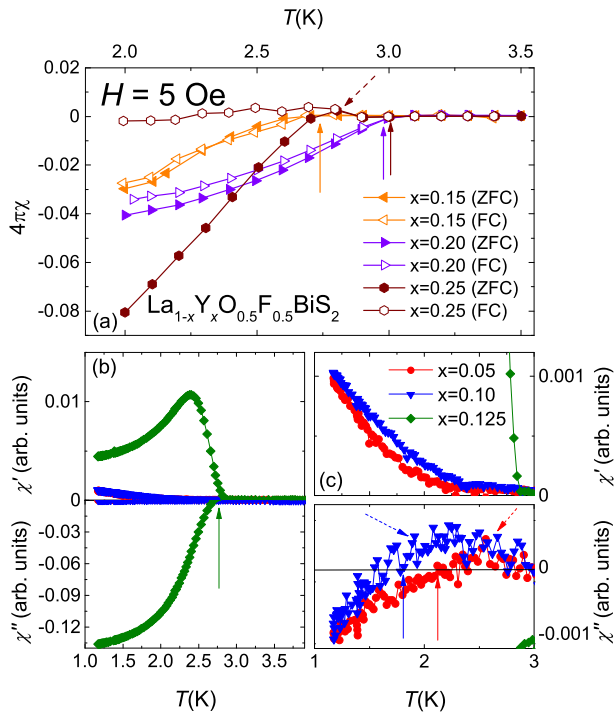


FIG. 4: (Color online) (a) Magnetic susceptibility χ_{dc} versus temperature T for $\text{La}_{1-x}\text{Y}_x\text{O}_{0.5}\text{F}_{0.5}\text{BiS}_2$ ($x = 0.15, 0.20$, and 0.25), measured in field cooled and zero-field cooled conditions. The solid arrows denote the superconducting critical temperature T_c and the dashed arrow emphasizes the presence of a small upturn. (b) and (c) Alternating current magnetic susceptibility χ_{ac} versus temperature T for $x = 0.05, 0.10$, and 0.125 . The solid and dashed arrows have the same meaning as in panel (a).

than 0.3 GPa, which is larger than the chemical pressure in the $x = 0.10$ compound (as will be discussed later). The semiconducting-like behavior is gradually suppressed for $x \geq 0.10$, which is similar to the results reported in pressure studies[26,27].

C. Magnetic Susceptibility

In order to characterize the observed superconductivity in the $\text{La}_{1-x}\text{Y}_x\text{O}_{0.5}\text{F}_{0.5}\text{BiS}_2$ system, temperature-dependent dc magnetic susceptibility measurements were performed under a 5 Oe magnetic field with both zero-field-cooled (ZFC) and field-cooled (FC) methods, and the results are displayed in Fig. 4 (a). We performed measurements on selected samples with $x = 0.15, 0.20$, and 0.25 which have superconducting transition temperatures T_c in the accessible temperature range of the MPMS. Clear diamagnetic signals were observed for each of these samples. The T_c values, determined by the temperatures at the onset of the diamagnetic signal, are indi-

TABLE I: Impurity phases $\text{La}_2\text{O}_2\text{S}$ and/or $\text{Y}_2\text{O}_2\text{S}$ by mass and superconducting volume fraction at 2 K along with T_c from ρ data for each concentration.

x	T_c (K)	Imp. (%)	V frac. (%)	Ref.
Parent	2.7	-	~ 6	[11]
	3.0	-	~ 13	[3]
	3.1	-	~ 60	[7]
	2.8	< 1	-	[This study]
0.05	2.5	~ 1	$\ll 1$	[This study]
0.10	1.8	~ 2	$\ll 1$	
0.125	2.9	~ 2	~ 11	
0.15	2.8	~ 3	~ 3	
0.20	3.1	~ 4	~ 4	
0.25	3.1	~ 8	~ 8	

cated by the solid arrows in Fig. 4 (a) and are in good agreement with those estimated from the electrical resistivity data. Alternating current magnetic susceptibility measurements for the samples with $x = 0.05, 0.10$, and 0.125 are shown in Figs. 4 (b) and (c). A clear signature of superconductivity was observed for $x = 0.125$ and the onset of a SC signal was observed for the $x = 0.05, 0.10$ samples. Though the transitions are not complete, we estimated superconducting shielding fractions of $\sim 13\%$ at 1.1 K for the $x = 0.125$ sample and $\sim 3\%$, $\sim 4\%$, and $\sim 8\%$ at 2 K for the $x = 0.15, 0.20$, and 0.25 samples, respectively. The weak signals for $x = 0.05, 0.10$ followed by increasing shielding fractions for $x \geq 0.125$ seem to correlate with the width of the transitions and the variation of the T_c values observed in electrical resistivity measurements. These shielding fractions are similar to reported values of $\sim 13\%$ and $\sim 6\%$ [3,11], but smaller than that of the highest value of $\sim 60\%$ [7]. The transition temperatures T_c from ρ , the amount of $\text{La}_2\text{O}_2\text{S}$ and/or $\text{Y}_2\text{O}_2\text{S}$ impurity phases by mass, and superconducting volume fractions at 2 K are summarized in Table I. These results imply that the volume fractions do not seem to correlate with Y concentrations or the amount of impurity phases; volume fractions more likely correlate with the transition temperatures and the broadness of transitions. The samples with $x = 0.05, 0.10$, and 0.25 exhibit a weak upturn indicated by dashed arrows in dc and ac susceptibility data in Fig. 4. This behavior is probably due to a small amount of paramagnetic impurities, as observed in other studies[7–10,13].

D. Specific Heat

To further investigate the superconducting properties of this system, measurements of the specific heat, C , were performed for the $x = 0.05$ and 0.25 samples in the temperature range from 1.8 K to 30 K. The results of these measurements are displayed in Fig. 5. Although the specific heat jump for the $x = 0.05$ sample is incomplete,

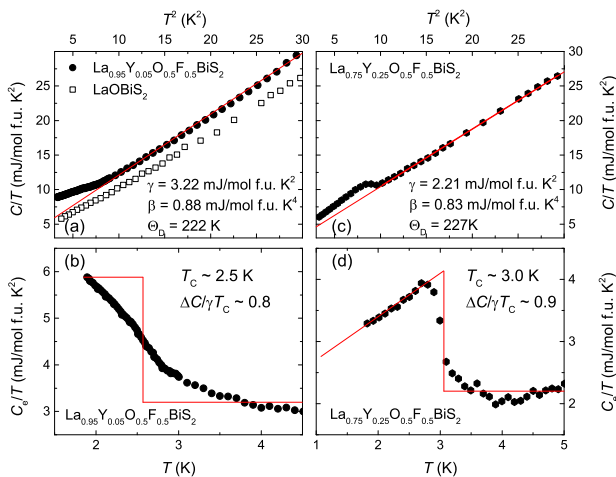


FIG. 5: (Color online) (a) and (c) Specific heat divided by temperature C/T versus temperature T for LaOBiS_2 , $\text{La}_{0.95}\text{Y}_{0.05}\text{O}_{0.5}\text{F}_{0.5}\text{BiS}_2$, and $\text{La}_{0.75}\text{Y}_{0.25}\text{O}_{0.5}\text{F}_{0.5}\text{BiS}_2$. The red lines represent the best fits to the equation $C(T)/T = \gamma + \beta T^2$ to the data which yield $\gamma = 3.22$ mJ/mol f.u. K^2 and $\Theta_D = 222$ K for $x = 0.05$ and $\gamma = 2.21$ mJ/mol f.u. K^2 and $\Theta_D = 227$ K for $x = 0.25$. (b) and (d) Plots of the electronic contribution to the specific heat divided by T , C_e/T , versus temperature T . Idealized entropy conserving constructions result in an estimate of $\Delta C/\gamma T_c = 0.8$ for $x = 0.05$ if we use $T_c = 2.5$ K from electrical resistivity measurements (see text) and $T_c = 3.0$ K and $\Delta C/\gamma T_c = 0.9$ for $x = 0.25$.

possibly due to its low T_c , we observed a broad upturn which is consistent with the T_c values obtained from ρ (2.5 K) and χ_{ac} (2.2 K), suggesting that this feature is associated with superconductivity. For the $x = 0.25$ sample, a clear specific heat jump is observed at $T_c \simeq 3.0$ K, in good agreement with the T_c values from ρ (3.1 K) and χ_{dc} (3.0 K). The appearance of a jump in C/T at T_c is strong evidence that the superconductivity for $x = 0.05$ and 0.25 is a bulk phenomenon. The specific heat at low temperature can be written,

$$C(T) = \gamma T + \beta T^3, \quad (2)$$

where the terms γT and βT^3 account for the electronic and phonon contributions, respectively. The data were fitted to this expression, yielding the electronic coefficient $\gamma = 3.22$ mJ/mol f.u. K^2 and the lattice coefficient $\beta = 0.88$ mJ/mol f.u. K^4 for the $x = 0.05$ sample and $\gamma = 2.21$ mJ/mol f.u. K^2 and $\beta = 0.83$ mJ/mol f.u. K^4 for the $x = 0.25$ sample. The best fits, shown in Figs. 5 (a) and (c), yield the fitting parameters listed in the figures. To obtain the ratios of the specific heat jump to γT_c , the lattice contributions were subtracted revealing the upturn and specific heat jump in Fig. 5 (b) and (d), respectively. Since the jump was incomplete for the $x = 0.05$ sample, a rough estimate of the ratio $\Delta C/\gamma T \sim 0.8$ was extracted from the size of the upturn and assuming $T_c \sim 2.5(1)$ K, as illustrated in Fig. 5 (b). This value is comparable to the value of 0.9 for the $x = 0.25$ sample, and both

of these are smaller than the value of 1.43 predicted by the weak-coupling Bardeen-Cooper-Schrieffer (BCS) theory of superconductivity; on the other hand, our values of γ , Θ_D , and $\Delta C/\gamma T$ are similar to $\gamma = 2.53$ mJ/mol f.u. K^2 , $\Theta_D = 221$ K, and $\Delta C/\gamma T = 0.94$ reported for $\text{LaO}_{0.5}\text{F}_{0.5}\text{BiS}_2$ [7].

It is noteworthy that the electronic specific heat behaves so differently from the predictions of the BCS theory. According to the BCS weak-coupling limit, the electronic specific heat below T_c decreases exponentially with decreasing temperature and almost reaches zero near $T_c/5$ [38]. In contrast to the BCS limit, our data for $x = 0.25$ are still larger than the normal state value at $T_c/2$, as seen in Fig. 5 (d). Similar behavior of specific heat was observed in previous studies[13,14]. Attempts to fit the specific heat data for $x = 0.25$ to a simple BCS expression for the low-temperature electronic specific heat, $C_e/\gamma T_c = 1.34(\Delta(0)/T)^{3/2}e^{-\Delta(0)/T}$ [39], where the exponential drop is determined by the zero-temperature energy gap, $\Delta(0)$, required the inclusion of additional temperature dependent and constant terms to satisfactorily fit the data (data and fits not shown). It is already known that these samples are not completely homogeneous, and such behavior suggests that part of the sample behaves as a bulk superconductor while the rest (the impurity phase portions of the sample) provide a non-superconducting contribution to C/T . The combination of these contributions presumably leads to the distinctly non-BCS temperature dependence we have observed in the behavior of $C_e(T)/T$ below T_c . We also note that there is a debate regarding whether or not BiS_2 -based superconductors actually exhibit conventional BCS superconductivity: weak electron-phonon coupling, a rather large value of $2\Delta/k_B T_c \sim 17$, giant superconducting fluctuations, and an anomalous semiconducting normal state have been considered for these compounds[22,40,41]. More investigations will be needed to determine the mechanism and nature of superconductivity in BiS_2 -based compounds.

IV. DISCUSSION

We summarize the results from ρ , χ_{dc} , χ_{ac} , and C measurements in a phase diagram of transition temperature T_c versus nominal yttrium concentration x , as shown in Fig. 6 (b). T_c decreases from 2.8 K to 1.8 K with increasing x until $x = 0.10$ and is roughly constant with a value of ~ 3.0 K for $x \geq 0.125$. T_c was found to decrease slightly in a study of the $\text{LaO}_{0.5}\text{F}_{0.5}\text{BiS}_2$ system under low applied pressures[26,27], as shown in the inset of Fig. 6 (b). This behavior of $T_c(P)$ resembles that of $T_c(x)$ in $\text{La}_{1-x}\text{Y}_x\text{O}_{0.5}\text{F}_{0.5}\text{BiS}_2$. This observation probably indicates that there is a relationship between T_c and crystal structure details. With that possibility in mind, we found that $T_c(x)$ is related to the lattice constant c (see Fig. 1 (b)) and the La-O-La bond angle (see Fig. 6 (a)).

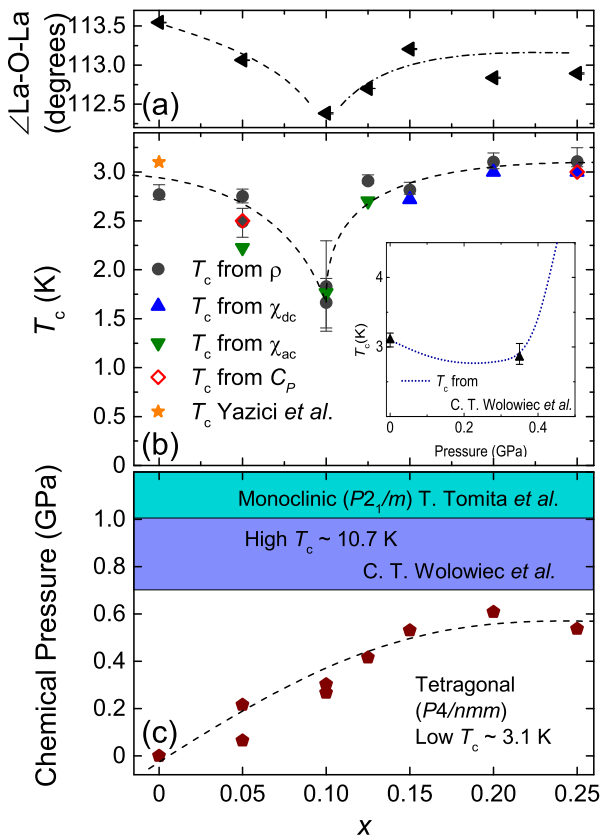


FIG. 6: (Color online) (a) La/Y-O/F-La/Y bond angle $\angle\text{La-O-La}$ versus nominal yttrium concentration x . (b) Superconducting transition temperature T_c versus nominal yttrium concentration x for the $\text{La}_{1-x}\text{Y}_x\text{O}_{0.5}\text{F}_{0.5}\text{BiS}_2$ system. The orange star is the maximum T_c obtained from electrical resistivity measurements of $\text{LaO}_{0.5}\text{F}_{0.5}\text{BiS}_2$ reported in Ref. [7]. The inset shows the behavior of T_c under applied pressure[27]. (c) Chemical pressure versus nominal yttrium concentration. Two regions with low T_c and high T_c (purple and blue regions) are separated by the reported critical pressure value $P_c \sim 0.7$ GPa[23,26,34]. The tetragonal (unfilled and purple regions) and monoclinic (blue region) phases are distinguished by the critical pressure $P_T \sim 1$ GPa for the structural phase transition[34].

Since the unit cell volume V decreases with increasing Y concentration until $x = 0.20$, the variation of T_c could be discussed in the context of chemical pressure. We adopted a value of the isothermal compressibility[34], $-d(V/V_0)/dP = 0.0089 \text{ GPa}^{-1}$ (bulk modulus is 112 GPa), where V and V_0 are the unit cell volumes with and without Y, respectively. A graph of chemical pressure versus the nominal Y concentration x is plotted in Fig. 6 (c) and the high T_c transition pressure $P_c \sim 0.7$ GPa[23,26] and structural phase transition pressure $P_T \sim 1$ GPa[34] are illustrated as purple and blue regions, respectively. Since $\text{LaO}_{0.5}\text{F}_{0.5}\text{BiS}_2$ with the tetragonal crystal structure ($P4/nmm$) is stable up to ~ 0.8 GPa and then experiences a complete structural phase tran-

sition above ~ 1.5 GPa, as discussed in previous studies of Tomita *et al.* and Mizuguchi *et al.*[3,34], the monoclinic phase is presumably responsible for the high- T_c superconducting phase. Our results show that chemical pressure increases with Y concentrations $0 \leq x \leq 0.20$ and saturates at a value of ~ 0.6 GPa at the solubility limit. In Fig. 6 (c), it is clear that the induced chemical pressure is insufficient to induce the high- T_c or the monoclinic phase. If the chemical pressure could be further increased, we expect that the high- T_c and monoclinic phases would be induced for $x \geq 0.20$. This is a simple explanation for why this system did not exhibit an enhancement of superconductivity.

Chemical pressure alone is unable to account for the suppression of superconductivity for $x \leq 0.10$. The lattice parameter c shows different behavior from the unit cell volume V . It increases slowly with increasing x to $x = 0.10$ and then decreases for $x \geq 0.15$ (see Fig. 1 (b)), in contrast to the monotonic increase of chemical pressure to $x = 0.20$. One possible scenario is that the La/Y-O/F-La/Y ($\angle\text{La-O-La}$) bond angle evolves with x . As shown in Fig. 6 (a), we observed a decrease of the bond angle for $0 \leq x \leq 0.10$ and then an increase for $0.125 \leq x \leq 0.25$, as obtained in our Rietveld refinements. Under applied pressure, the lattice parameters a and c of $\text{LaO}_{0.5}\text{F}_{0.5}\text{BiS}_2$ decrease continuously until a structural phase transition is induced near 1 GPa[34]. However, chemical pressure is insufficient to induce the structural phase transition. The suppression and subsequent enhancement of superconductivity with x are probably related to the variation of the lattice parameter c , suggesting that the superconducting transition temperature is tuned by c in BiS_2 -based systems, which is consistent with the conclusions of another recent experimental study[42]. The width of the superconducting transition, energy gap values, and superconducting volume fractions also seem to vary systematically with the lattice parameter c .

To the best of our knowledge, studies on BiS_2 -based compounds still report difficulties synthesizing homogeneous samples; superconducting critical temperatures for the same systems show perceptible discrepancies between studies[3,4,6–10]. Also, the lattice parameters or volumes of the same compounds vary for different studies, as seen in Fig. 2(a). Often, the systematic chemical substitution studies of the same systems have different phase diagrams[4,6,8,12,15,16]. Sometimes T_c does not change and seems to be independent of substituent concentrations until a solubility limit emerges, even though both parent compounds are stable and can be synthesized[13].

These discrepancies in the lattice parameters, phase diagrams, and transition temperatures T_c between studies might have one or more possible causes: Fluorine substitution studies for $\text{LnO}_{1-x}\text{F}_x\text{BiS}_2$ ($\text{Ln} = \text{La}, \text{Ce}, \text{Nd}$)[3,4,6] showed variations of lattice parameters and T_c for similar nominal fluorine concentrations. Because of the quantitative inaccuracy of EDX measurements for these materials[41], it is difficult to estimate the ex-

act amount of fluorine in BiS₂ compounds. Thus, it is probable that the actual and nominal fluorine ratio could be different, resulting in differences of lattice parameters and T_c . On the other hand, recent studies of angle-resolved photoemission spectroscopy (ARPES) and optical spectroscopy[43,44] on Nd(O,F)BiS₂ report rather small electron doping levels of roughly 7 % per Bi site, which is smaller than the high electron doping level, $x \sim 0.5$, expected from theoretical studies. A low electron doping level, intrinsic structural instabilities[22], and possible bismuth deficiencies[45] in BiS₂ compounds also complicate our ability to compare results from different studies and combinations of those factors possibly yield such disparities in crystallographic and superconducting properties between studies. In order to advance our understanding of superconductivity in BiS₂-based compounds, these materials issues must be addressed.

V. CONCLUDING REMARKS

We have studied the effect of partial chemical substitution of yttrium for lanthanum in the superconducting LaO_{0.5}F_{0.5}BiS₂ system. We synthesized polycrystalline

samples of La_{1-x}Y_xO_{0.5}F_{0.5}BiS₂ up to $x = 0.40$ and observed a solubility limit near $x = 0.20$. All samples crystallized in the CeOBiS₂-type structure. The physical properties of the system were investigated via electrical resistivity, dc and ac magnetic susceptibility, and specific heat measurements. We found a correlation between the lattice constant c , the La-O-La bond angle, and the critical temperature T_c . The chemical pressure induced by yttrium substitution for lanthanum is insufficient to induce the high- T_c and/or the structural phase transitions observed in measurements of LaO_{0.5}F_{0.5}BiS₂ under applied pressure.

Acknowledgments

This work was supported by the US Air Force Office of Scientific Research - Multidisciplinary University Research Initiative under Grant No. FA 9550-09-1-0603 (superconductivity search), the US Department of Energy under Grant No. FG0204-ER46105 (characterization and physical properties measurements), and the National Science Foundation under Grant No. DMR 1206553 (low-temperature measurements).

-
- * Corresponding Author: mbmaple@ucsd.edu
- ¹ Y. Mizuguchi, H. Fujihisa, Y. Gotoh, K. Suzuki, H. Usui, K. Kuroki, S. Demura, Y. Takano, H. Izawa, and O. Miura, Phys. Rev. B **86**, 220510 (2012).
 - ² S. K. Singh, A. Kumar, B. Gahtori, Shruti, G. Sharma, S. Patnaik, and V. P. S. Awana, J. Am. Chem. Soc. **134**, 16504 (2012).
 - ³ Y. Mizuguchi, S. Demura, K. Deguchi, Y. Takano, H. Fujihisa, Y. Gotoh, H. Izawa, and O. Miura, J. Phys. Soc. Jpn. **81**, 114725 (2012).
 - ⁴ S. Demura, Y. Mizuguchi, K. Deguchi, H. Okazaki, H. Hara, T. Watanabe, S. J. Denholme, M. Fujioka, T. Ozaki, H. Fujihisa, et al., J. Phys. Soc. Jpn. **82**, 033708 (2013).
 - ⁵ K. Deguchi, Y. Mizuguchi, S. Demura, H. Hara, T. Watanabe, S. J. Denholme, M. Fujioka, H. Okazaki, T. Ozaki, H. Takeya, et al., Europhys.Lett. **101**, 17004 (2013).
 - ⁶ J. Xing, S. Li, X. Ding, H. Yang, and H.-H. Wen, Phys. Rev. B **86**, 214518 (2012).
 - ⁷ D. Yazici, K. Huang, B. D. White, A. H. Chang, A. J. Friedman, and M. B. Maple, Philos. Mag. **93**, 673 (2012).
 - ⁸ R. Jha and V. P. S. Awana, J. Sup. Novel Mag. **27**, 1 (2014).
 - ⁹ R. Jha, A. Kumar, S. Kumar Singh, and V. P. S. Awana, J. Appl. Phys. **113**, 056102 (2013).
 - ¹⁰ R. Jha, A. Kumar, S. K. Singh, and V. P. S. Awana, J. Sup. Novel Mag. **26**, 499 (2013).
 - ¹¹ V. P. S. Awana, A. Kumar, R. Jha, S. Kumar Singh, A. Pal, Shruti, J. Saha, and S. Patnaik, Solid State Commun. **157**, 21 (2013).
 - ¹² R. Jha and V. P. S. Awana, Mater. Res. Express **1**, 016002 (2014).
 - ¹³ D. Yazici, K. Huang, B. D. White, I. Jeon, V. W. Burnett, A. J. Friedman, I. K. Lum, M. Nallaiyan, S. Spagna, and M. B. Maple, Phys. Rev. B **87**, 174512 (2013).
 - ¹⁴ X. Lin, X. Ni, B. Chen, X. Xu, X. Yang, J. Dai, Y. Li, X. Yang, Y. Luo, Q. Tao, et al., Phys. Rev. B **87**, 020504 (2013).
 - ¹⁵ Y. Li, X. Lin, L. Li, N. Zhou, X. Xu, C. Cao, J. Dai, L. Zhang, Y. Luo, W. Jiao, et al., Supercond. Sci. Technol. **27**, 035009 (2014).
 - ¹⁶ H. Sakai, D. Kotajima, K. Saito, H. Wadati, Y. Wakisaka, M. Mizumaki, K. Nitta, Y. Tokura, and S. Ishiwata, J. Phys. Soc. Jpn. **83**, 014709 (2014).
 - ¹⁷ H. Usui, K. Suzuki, and K. Kuroki, Phys. Rev. B **86**, 220501 (2012).
 - ¹⁸ X. Wan, H.-C. Ding, S. Y. Savrasov, and C.-G. Duan, Phys. Rev. B **87**, 115124 (2013).
 - ¹⁹ Shruti, P. Srivastava, and S. Patnaik, J. Phys.: Condens. Matter **25**, 339601 (2013).
 - ²⁰ G. Lamura, T. Shiroka, P. Bonfa, S. Sanna, R. De Renzi, C. Baines, H. Luetkens, J. Kajitani, Y. Mizuguchi, O. Miura, et al., Phys. Rev. B **88**, 180509 (2013).
 - ²¹ T. Yildirim, Phys. Rev. B **87**, 020506 (2013).
 - ²² J. Lee, M. B. Stone, A. Huq, T. Yildirim, G. Ehlers, Y. Mizuguchi, O. Miura, Y. Takano, K. Deguchi, S. Demura, et al., Phys. Rev. B **87**, 205134 (2013).
 - ²³ H. Kotegawa, Y. Tomita, H. Tou, H. Izawa, Y. Mizuguchi, O. Miura, S. Demura, K. Deguchi, and Y. Takano, J. Phys. Soc. Jpn. **81**, 103702 (2012).
 - ²⁴ G. Kalai Selvan, M. Kanagaraj, S. Esakki Muthu, R. Jha, V. P. S. Awana, and S. Arumugam, Phys. Status Solidi R **7**, 510 (2013).
 - ²⁵ G. Kalai Selvan, M. Kanagaraj, R. Jha, V. P. S. Awana, and S. Arumugam, arXiv:1307.4877 (2013).
 - ²⁶ C. T. Wolowiec, D. Yazici, B. D. White, K. Huang, and

- M. B. Maple, Phys. Rev. B **88**, 064503 (2013).
- ²⁷ C. T. Wolowiec, B. D. White, I. Jeon, D. Yazici, K. Huang, and M. B. Maple, J. Phys.: Condens. Matter **25**, 422201 (2013).
- ²⁸ J. Kajitani, K. Deguchi, A. Omachi, T. Hiroi, Y. Takano, H. Takatsu, H. Kadowaki, O. Miura, and Y. Mizuguchi, Solid State Commun. **181**, 1 (2014).
- ²⁹ K. Mori, Y. Isikawa, K. Kobayashi, M. Sasakawa, and K. Sato, Physica B+C **148**, 465 (1987).
- ³⁰ T. F. Liao, H. H. Sung, K. J. Syu, and W. H. Lee, Solid State Commun. **149**, 448 (2009).
- ³¹ H. Mizoguchi, T. Kuroda, T. Kamiya, and H. Hosono, Phys. Rev. Lett. **106**, 237001 (2011).
- ³² P. M. Shirage, K. Miyazawa, H. Kito, H. Eisaki, and A. Iyo, Phys. Rev. B **78**, 172503 (2008).
- ³³ M. Tropeano, C. Fanciulli, F. Canepa, M. R. Cimberle, C. Ferdeghini, G. Lamura, A. Martinelli, M. Putti, M. Vignolo, and A. Palenzona, Phys. Rev. B **79**, 174523 (2009).
- ³⁴ T. Tomita, M. Ebata, H. Soeda, H. Takahashi, H. Fujihisa, Y. Gotoh, Y. Mizuguchi, H. Izawa, O. Miura, S. Demura, et al., J. Phys. Soc. Jpn. **83**, 063704 (2014).
- ³⁵ A. C. Larson and R. B. V. Dreele, Los Alamos National Laboratory Report (1994).
- ³⁶ B. Toby, J. Appl. Crystallogr. **34**, 210 (2001).
- ³⁷ R. D. Shannon, Acta Cryst. A **32**, 751 (1976).
- ³⁸ F. Bouquet, Y. Wang, R. A. Fisher, D. G. Hinks, J. D. Jorgensen, A. Junod, and N. E. Phillips, Europhys. Lett. **56**, 856 (2001).
- ³⁹ N. W. Ashcroft and N. D. Mermin, *Solid State Physics* (Saunders College, Philadelphia, 1976).
- ⁴⁰ S. Li, H. Yang, D. Fang, Z. Wang, J. Tao, X. Ding, and H. Wen, Sci. China-Phys. Mech. Astron. **56**, 2019 (2013).
- ⁴¹ J. Liu, D. Fang, Z. Wang, J. Xing, Z. Du, S. Li, X. Zhu, H. Yang, and H.-H. Wen, Europhys. Lett. **106**, 67002 (2014).
- ⁴² J. Kajitani, K. Deguchi, T. Hiroi, A. Omachi, S. Demura, Y. Takano, O. Miura, and Y. Mizuguchi, J. Phys. Soc. Jpn. **83**, 065002 (2014).
- ⁴³ L. K. Zeng, X. B. Wang, J. Ma, P. Richard, S. M. Nie, H. M. Weng, N. L. Wang, Z. Wang, T. Qian, and H. Ding, arXiv:1402.1833 (2014).
- ⁴⁴ X. B. Wang, S. M. Nie, H. P. Wang, P. Zheng, P. Wang, T. Dong, H. M. Weng, and N. L. Wang, Phys. Rev. B **90**, 054507 (2014).
- ⁴⁵ Z. R. Ye, H. F. Yang, D. W. Shen, J. Jiang, X. H. Niu, D. L. Feng, Y. P. Du, X. G. Wan, J. Z. Liu, X. Y. Zhu, et al., Phys. Rev. B **90**, 045116 (2014).